Efficient Line Beam Scanning Based on a Hybrid Optical Phased Array Rendering Flexible Field-of-Views

Chenxi Wang, Eun-Su Lee, Jinung Jin, Bishal Bhandari, *Graduate Student Member, IEEE*, Ji-Yeong Gwon, Menglong Luo, Jin-Moo Heo, Seong-Hyeon Ju, Sung-Yong Ko, Jung-O Son, Min-Cheol Oh, and Sang-Shin Lee

***Abstract*—Conventional OPAs incorporating a diffraction grating were mainly developed to achieve a two-dimensional spot beam-based scan, which inevitably requires a wide range of wavelength tuning, leading to unaffordable complexity and limited scanning speed. In this study, we demonstrate a hybrid OPA that capitalizes on a silicon nitride line beam emitter based on tapered waveguides array, which facilitates efficient line beam scanning exhibiting flexible vertical field-of-views (FOVs) at a wavelength of 1550 nm. The line beam is horizontally scanned by driving an array of hybrid-integrated thermo-optic polymer phase modulators. The vertical FOV can be flexibly adjusted by varying the tip widths of the tapers and thus the angular divergence of emitted beams, leading to flexible FOVs ranging from 30° × 14° to 30° × 47°. A lens module is particularly devised and tethered to the OPA, thereby further tailoring and amplifying the FOVs along vertical and horizontal directions. The proposed hybrid OPA in conjunction with a lens module was practically manufactured to efficiently substantiate desired line beam scanning, achieving FOVs ranging from 51° × 0.6° to 51° × 10.3°. The developed line-beam-based OPA is anticipated to play an integral role in embodying an advanced LiDAR system featuring fast beam scanning.**

***Index Terms*—Optical phased array, hybrid-integrated circuit, light detection and ranging.**

I. Introduction

OPTICAL phased arrays (OPAs) have attracted significant interest in recent years because they offer fast inertia-free beam scanning, flexible non-mechanical beam forming, and compatibility with large-scale complementary metal-oxide semiconductor (CMOS) processes [1], [2], [3], [4], [5], [6]. These advantages have led to their potential use in a broad range of advanced applications, including light detection and ranging (LiDAR), free-space communication, and holographic displays. Currently, OPAs are preferred as beam scanning devices because they can offer high precision, a large field-of-view (FOV), and low power consumption [7], [8], [9]. Typically, OPA structures based on a surface grating, which resort to grating antenna arrays, were reported as a feasible candidate for use in conventional 2D beam scanners. With the aid of grating waveguide arrays, these devices realize 2D beam scanning by tuning the wavelength along the vertical direction and inducing a phase gradient across the grating waveguide array along the horizontal direction. However, 2D raster beam scanning requires substantial time, considering each row and column need to be scanned individually over a specific area [13], [14], [15], [16], [17], [18], [19]. In addition, the combination of a costly tunable laser required for vertical beam scanning, high-precision fabrication conditions, and extra loss due to the surface relief grating hinders the development of the conventional grating-incorporated OPA for the advanced LiDAR schemes. In this context, OPAs allowing for line beam scanning have emerged as a prominent platform owing to their faster scanning speed, fixed operation wavelength, and higher emission efficiency compared with 2D scanning based on a point beam [20], [21], [22], [23].

In the meantime, silicon photonics has been regarded as an outstanding platform for the design of OPAs owing to its CMOS compatibility, low cost, and high refractive index contrast. It is however known that the output power that can be dealt with by silicon-based devices is adversely affected by nonlinear absorption effects, such as free carrier absorption and two-photon absorption [4], [5]. As a result, silicon photonic chips are unable to handle higher-power light, which restricts their use for long-distance transmission. Silicon nitride (SiN) has been highlighted as an alternative CMOS platform owing to its high-power handling capacity, lower nonlinearity, and wider transparency spanning the visible and infrared regions in comparison to that of silicon [10], [11], [12], [13], [14], [15], [17], [24]. However, SiN is not recommended for phase shifting because of its lower thermo-optic (TO) coefficient, which increases

Manuscript received 19 November 2022; revised 1 February 2023; accepted 13 February 2023. Date of publication 16 February 2023; date of current version 24 February 2023. This work was supported by the Challengeable Future Defense Technology Research and Development Program of Agency for Defense Development in 2022 under Grant 912905601. *(Chenxi Wang and Eun-Su Lee contributed equally to this work.) (Corresponding authors: Sang-Shin Lee; Min-Cheol Oh.)*

Chenxi Wang, Bishal Bhandari, Ji-Yeong Gwon, Menglong Luo, Jin-Moo Heo, and Sang-Shin Lee are with the Department of Electronic Engineering, Kwangwoon University, Seoul 01897, South Korea (e-mail: wangchenxi70@gmail.com; photonicsbishal@gmail.com; skaans78@naver.com; menglongluo1995@gmail.com; hjm3937@kw.ac.kr; slee@kw.ac.kr).

Eun-Su Lee, Jinung Jin, and Min-Cheol Oh are with the Department of Electronic Engineering, Pusan National University, Busan 46241, South Korea (e-mail: ensulee@pusan.ac.kr; jinung@pusan.ac.kr; mincheoloh@pusan.ac.kr).

Seong-Hyeon Ju, Sung-Yong Ko, and Jung-O Son are with the i3system, Daejeon, Yuseong-gu 34113, South Korea (e-mail: seonghyeon.joo@i3system.com; hallaksy0@gmail.com; joson@i3system.com).

Digital Object Identifier 10.1109/JPHOT.2023.3245623

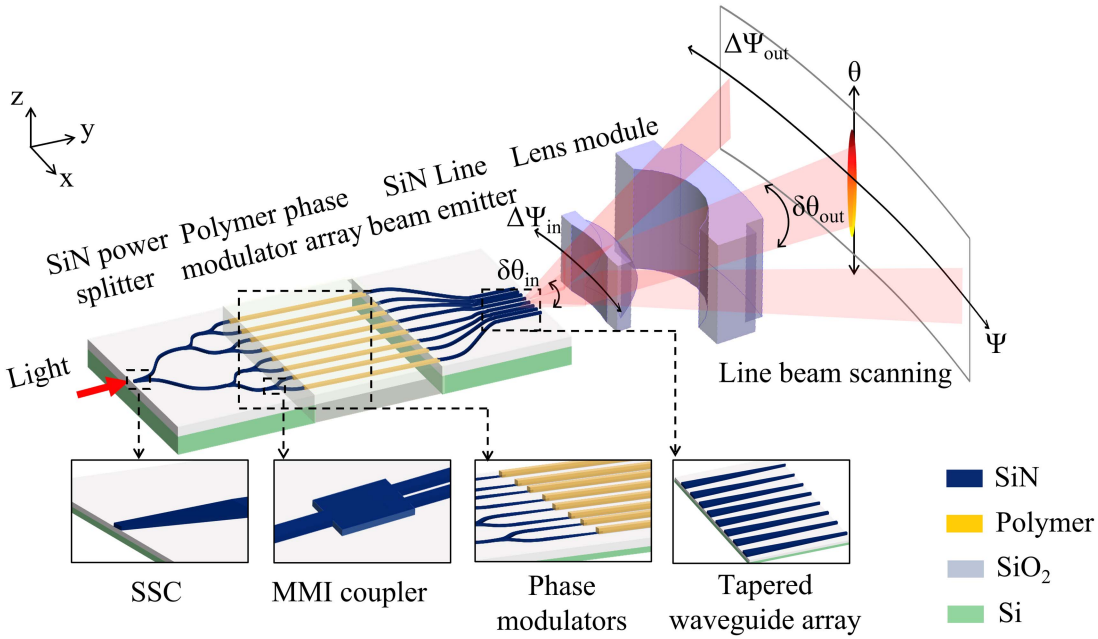

Fig. 1. Schematic configuration of the proposed beam transmitter, which consists of a hybrid OPA combined with a lens module, enabling efficient line beam scanning with flexible FOVs.

power consumption. Hence, a hybrid integrated configuration incorporating other materials exhibiting a high TO coefficient is to be deployed to mitigate the issue of power consumption. In this study, a hybrid integrated OPA capitalizing on a line beam emitter, comprising an array of tapered waveguides in SiN, has been implemented to execute efficient line beam scanning, substantiating flexible FOVs at a fixed wavelength of 1550 nm. An array of polymer phase modulators was integrated with a SiN power splitter and line beam emitter, which is responsible for the horizontal beam scanning by inducing phase gradients. The line beam emitter made of SiN, incorporating arrayed tapered waveguides with varying tip widths, gives rise to flexible vertical FOVs in accordance with the mode field diameter (MFD) at the end facet of the waveguides. The proposed hybrid OPAs have been rigorously designed and fabricated to scrutinize the emission response in terms of line beam scanning. Next, a lens module has been combined with the hybrid OPA to further tailor and enhance the FOVs along the vertical and horizontal directions, respectively. It is stated that the FOVs are dictated by the vertical beamwidth and horizontal scanning range. An OPA transmitter, which consists of the hybrid OPA in conjunction with the lens module, was finally concocted to execute one-dimensional line beam scanning, giving rise to an adjustable FOV.

II. Design of the Proposed Hybrid OPA Providing Line Beams Enabling Flexible FOVs

The proposed hybrid OPA rendering line beam scanning comprises a SiN power splitter and line beam emitter made of SiN, in conjunction with a phase modulator array in polymer, as illustrated in Fig. 1. A spot size converter (SSC) conveys incident light from a laser source to the SiN power splitter, which is based on six stages of serially cascaded 1×2 multimode interference (MMI) couplers. An array of phase modulators, which are appended to the preceding SiN power splitter via a similar SSC, is subsequently connected to a SiN line beam emitter, which draws upon uniformly spaced tapered waveguides. Finally, a lens module that is externally combined with the OPA is introduced to tailor the vertical beamwidth and concurrently expand the horizontal scanning range.

As for the proposed hybrid OPA, incident light fed by the SSC is first evenly split into 64 waveguides through the power splitter, whose output is subsequently delivered to the phase modulators via similar types of SSCs. They are implemented in the form of a linearly tapered waveguide with a length of 1500 μm and a tip width of 200 nm, thereby mimicking the MFD of the polymer waveguide. The phase of the propagating light is manipulated to induce a constant phase gradient across the channels. The phase-modulated guided mode then impinges upon the line beam emitter, which comprises the tapered waveguide, eventually steering the line beam along the Ψ-direction in response to the phase gradient, exhibiting flexible FOVs along the θ-direction. A lens module is combined with the OPA, with the aim of controlling the vertical FOV and simultaneously expanding the beam scanning range along the horizontal Ψ-direction. As indicated in Fig. 1, $\delta\theta_{\mathrm{in}}$ and $\Delta\Psi_{\mathrm{in}}$ denote the vertical beamwidth and horizontal scanning range of the beam emanating from the hybrid OPA, respectively, while $\delta\theta_{\mathrm{out}}$ and $\Delta\Psi_{\mathrm{out}}$ represent the vertical beamwidth and horizontal scanning range of the output line beam exiting from the lens module, respectively.

For a single-mode SiN waveguide, a core with a thickness of 500 nm and width of 1 μm was adopted to achieve appropriate mode confinement, leading to low propagation/bending losses [12]. However, the beamwidth along the θ-direction, hinging on the dimension of the end facet of the waveguides constituting the line beam emitter, is deemed to be excessively large and

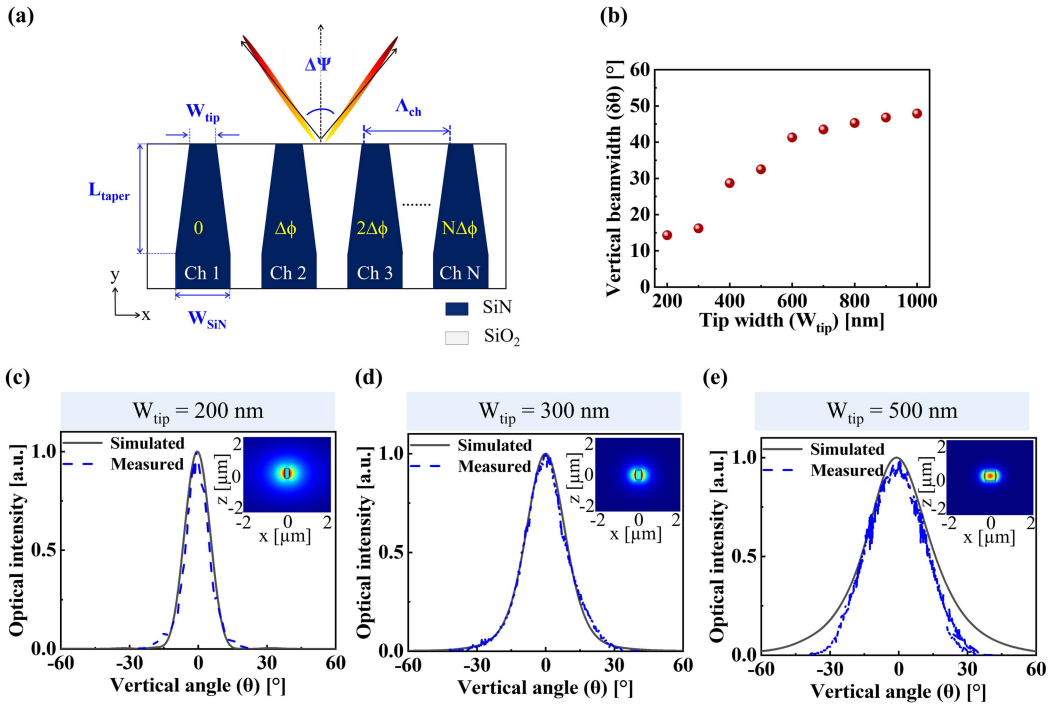

Fig. 2. (a) Schematic of the line beam emitter based on an array of tapered waveguides. (b) Calculated $\delta\theta$ for W_{tip} ranging from 0.2 μm to 1 μm. Comparison of simulated and measured results in terms of the beamwidth along the vertical direction for W_{tip} = (c) 0.2 μm, (d) 0.3 μm, and (e) 0.5 μm. Images in the inset sketch the corresponding electric-field profiles.

adversely affects the operation distance as a scanning device. Considering a waveguide may be linearly tapered to alter the MFD, a line beam emitter incorporating an array of tapered waveguides has been conceived. The line beam emitter was designed and analyzed using a simulation tool based on the 3D finite difference time domain (FDTD) (Lumerical Inc.). Fig. 2(a) shows a schematic of the designed 2D-modeled line beam emitter, where W_{tip}, L_{taper}, $\Delta\varphi$, and $\Delta\Psi$ indicate the width of the waveguide tip, taper length, applied phase difference between adjacent channels, and horizontal scanning range, respectively. For a uniform waveguide array, the scanning angle Ψ is governed by the applied phase difference $\Delta\varphi$, in accordance with $\sin\Psi = \lambda\Delta\varphi / (2\pi\Lambda_{ch})$. The horizontal beamwidth is determined by the entire span of the array, tantamount to $N\Lambda_{ch}$, where λ, N, and Λ_{ch} are the wavelength, number of channels, and channel spacing (period), respectively. A uniform waveguide array consisting of 64 channels was constructed with a period of 3 μm. Owing to the reduced tip width (W_{tip}) of the taper, the confinement of the traveling mode is weakened along the propagation direction, ultimately resulting in an enlarged MFD. For a SiN waveguide with a 500-nm-thick core, the MFD, which was as small as 0.8 $\times$ 0.7 μm^2 for W_{tip} = 1 μm, was enlarged to be 2.1 $\times$ 2.2 μm^2 for W_{tip} = 0.2 μm. The electric-field beam profiles were computed through a simulation tool, MODE Solutions (Lumerical Inc.). The vertical beamwidth ($\delta\theta$) of the tapered waveguide was explored in terms of W_{tip}, as shown in Fig. 2(b). For W_{tip} running from 0.2 μm to 1 μm, the vertical FOV of the corresponding line beam was changed from 14° to 47° depending on the corresponding MFD of the emerging line beam. As expected, the angular beamwidth was substantially diminished in the vertical direction with decreasing W_{tip}. Fig. 2(c), (d), and (e) show the simulation and measurement results in terms of the beamwidth along the θ-direction. The measured $\delta\theta$ was 13°, 20°, and 32° for an OPA with W_{tip} = 200, 300, and 500 nm, respectively. The detailed fabrication and experimentation procedure will be described in Section III.

To further inspect the emission response of the proposed OPA, L_{taper} and W_{tip} were selected to be 100 μm and 300 nm, respectively, by scrutinizing the vertical beamwidth and power loss of an elemental tapered waveguide with respect to the tip width. It is noted that two adjacent tapered waveguides with a 300-nm-wide tip and 100-μm length, as adopted for the proposed line beam emitter, was observed to incur an optical crosstalk of ~13 dB due to their gradually enlarged MFD along the propagation direction. However, it was analytically confirmed that the performance of our line beam emitter was hardly adversely affected in terms of beamforming and beam scanning. Fig. 3(a) and (b) show the polar far-field beam pattern in relation to the OPA for applied phase differences of $\Delta\varphi$ = 0° and 180°, respectively. For a scanning angle at 0°, a pair of tenuous grating lobes were monitored to be positioned at $\Psi = \pm 31.1°$ as expected. The grating lobes, which occur regularly on both sides of the main lobe, were determined in accordance with $\sin\Psi_{grating} = \pm m\lambda/\Lambda_{ch}$, where m, λ, and Λ_{ch} are the diffraction order of grating, wavelength, and channel spacing, respectively. Fig. 3(c) shows the horizontal cross-section of the emitted beam when $\Delta\varphi$ was changed from –120° to 180° in steps of 60°. The achievable maximum scanning range was observed to be ~30° with a horizontal full width at half maximum (FWHM) of ~0.4°. The main lobe intensity dropped by ~3.3 dB during horizontal scanning, which is governed by

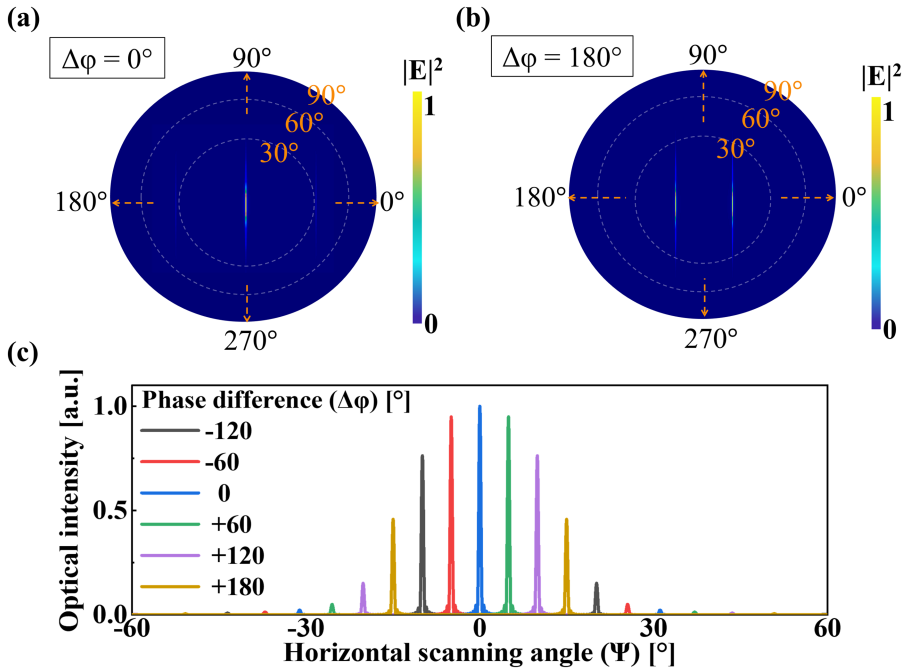

Fig. 3. Polar far-field patterns emerging from the OPA for $\Delta\varphi$ of (a) 0° and (b) 180°. (c) Simulated beam profiles along the horizontal direction.

the aperture of a single tapered waveguide. The power variation of main lobe during scanning is presumed to be alleviated by capitalizing on a gap cavity [21]. It is implied that the tapered waveguide structure could be incorporated into the line beam emitter, providing FOVs of 30° × 20° ($\Psi \times \theta$).

When it comes to the lens module, a pair of lenses were attempted and inspected to adjust and enhance the FOVs along the vertical and horizontal directions, respectively. The lens module was rigorously designed with the aid of LightTools (Synopsys Inc.). Fig. 4(a) illustrates a schematic of the designed lens module and its ray-optic behavior, where lenses V and H, with focal lengths f_1 and f_2, respectively, are cascaded in series under a fixed distance (d_2) of 19.5 mm. As shown in Fig. 4(a)–(i), line beams originating from the hybrid OPA are focused by the first vertical lens (lens V), resulting in a diminished vertical beamwidth ($\delta\theta_{\text{out}}$), while a reduction factor ($\delta\theta_{\text{in}}/\delta\theta_{\text{out}}$) depends on the working distance (d_1) of lens V. A line beam with a diminished $\delta\theta_{\text{out}}$ then enters the second horizontal lens (lens H), which is responsible for amplifying the horizontal scanning range by a factor of M, which is equivalent to $\Delta\Psi_{\text{out}}/\Delta\Psi_{\text{in}}$, as shown in Fig. 4(a)–(ii). The input vertical beamwidth, output vertical beamwidth, and input and output horizontal scanning angles are denoted by $\delta\theta_{\text{in}}$, $\delta\theta_{\text{out}}$, Ψ_{in} and Ψ_{out}, respectively. To examine the stability of $\delta\theta_{\text{out}}$ as well as the amplification of the horizontal scanning range, the working distance (d_1) between the OPA and lens V was fixed at 2.5 mm. Ψ_{out} and $\delta\theta_{\text{out}}$ relating to the output beam were checked in terms of Ψ_{in}, as shown in Fig. 4(b). It was hence found that the designed lens module could enlarge the horizontal scanning range from ±15° to ±25.5°, translating into a magnification factor of M = 1.7 ($\Psi_{\text{out}}/\Psi_{\text{in}}$). $\delta\theta_{\text{out}}$ was observed to remain in the vicinity of 5.0° during beam scanning.

As regards the beam convergence of the proposed lens module, the relationship between $\delta\theta_{\text{out}}$ and d_1 was investigated in simulation and experiment, as shown in Fig. 5. The output vertical beamwidth ($\delta\theta_{\text{out}}$) was adjusted from 10.3° to 0.6° by altering the working distance between the OPA chip and lens module from $d_1 = 1$ to 4 mm. $\delta\theta_{\text{out}}$ was found to decrease with d_1 at a rate of ∼3.2°/mm, as expected. The inset images reveal the captured beam profiles for $d_1 = 2.2$ and 3.8 mm, signifying that the proposed hybrid OPA linked to the lens module gives rise to FOVs ($\Psi \times \theta$) ranging from 51° × 10.3° to 51° × 0.6°, which is advantageous for LiDAR applications in terms of scanning speed and areal coverage. It is particularly stated that the structural formula of the lens surface of concern is given by:

$$z\ (x,y) = \frac{(C_x)x^2 + (C_y)\,y^2}{1+\sqrt{1-(1+k_x)\,C_x^2x^2-(1+k_y)\,C_y^2y^2}} + \sum_{n=1}^{3} A_{2n}x^{2n}$$

where k, C, f, and A represent the conic constant, surface curvature, focal length, and symmetric higher-order coefficients of the lens surface, respectively. The design parameters of the lens module are presented in Table I in detail.

III. Implementation of the Designed OPA Transmitter and Its Characterization

The designed hybrid integrated OPA chip and lens module were practically prepared and assembled to establish an OPA transmitter, providing a line beam for 1D scanning. As depicted in Fig. 1, a line beam emitter in SiN, based on an array of tapered waveguides with a tip width of 300 nm, was linked with a polymeric phase modulator chip. Fig. 6(a) displays the packaged OPA transmitter, which includes the input fiber, power splitter, line beam emitter, and phase modulator array. It is mentioned that a thermo-electric cooler (TEC) placed on the printed circuit board is used to adaptively tailor the ambient temperature in

TABLE I
DESIGN PARAMETERS OF THE LENS MODULE

Parameters	Surface	(k_x, k_y)	(C_x, C_y)	f (mm)	Higher-order coefficient (A_{2n})		
					n = 1	n = 2	n = 3
Lens V	Front	(0, 0)	(0.09, 0)	5.3	0	-8e–4	0
	Rear	(0, -1.5)	(0.13, 0.29)	9.6	0	0	0
Lens H	Front	(-0.1, 0)	(0.14, 0)	17	0	5e–5	0
	Rear	(-4.5, 0)	(0.02, 0)	20	0	3.15e–5	-5.5e–8

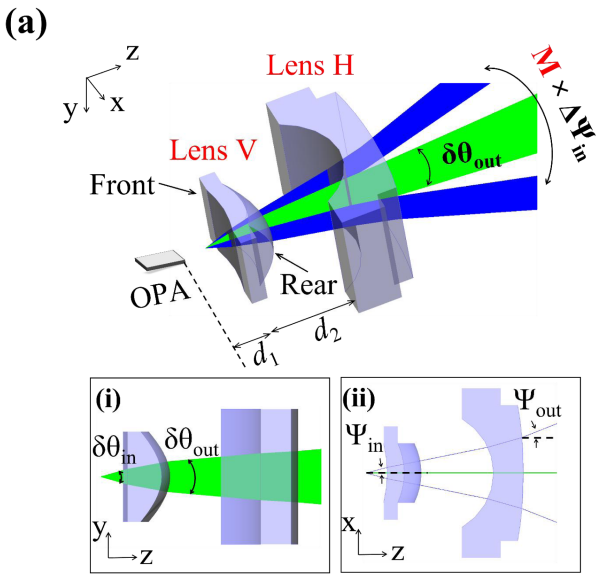

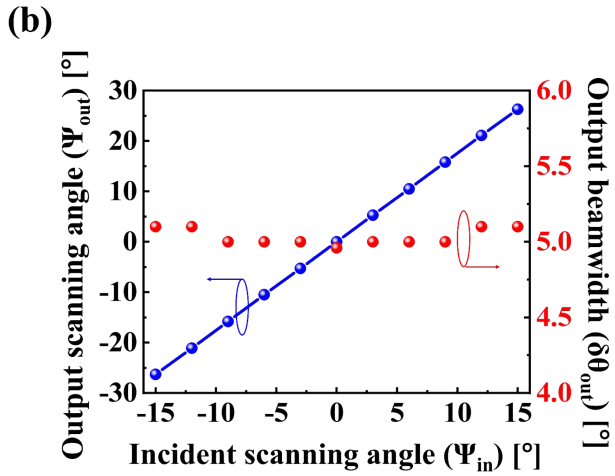

Fig. 4. (a) Schematic of the designed lens module, indicating the ray tracing results pertaining to (i) the vertical and (ii) horizontal lenses. (b) Calculated steering angle (Ψ_{out}) of the outgoing main beam and the output beamwidth along the vertical direction ($\delta\theta_{out}$) when incident angle (Ψ_{in}) changes from −15° to 15°.

the neighborhood of the phase modulators, thereby achieving a stable operation of the devices. Details of the completed hybrid OPA are shown in Fig. 6(b). It is remarked that the SSC was incorporated into the SiN waveguides to improve the coupling loss at the interface between the SiN and polymer chips. From the perspective of their high TO coefficients and low thermal conductivities, polymeric phase modulators were particularly designed and applied to impart a phase gradient

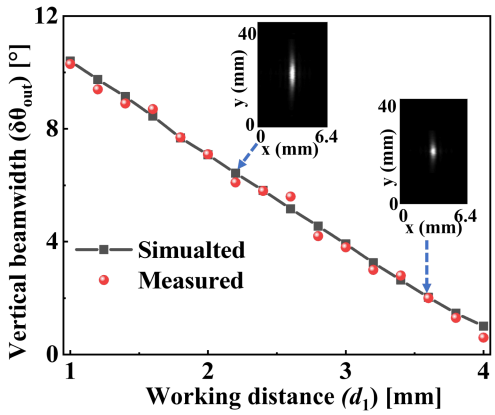

Fig. 5. Comparison of the measured and simulated output vertical beamwidth ($\delta\theta_{out}$) as a function of the working distance (d_1) of the lens module. The far-field profiles in the inset correspond to d_1 of 2.2 and 3.8 mm.

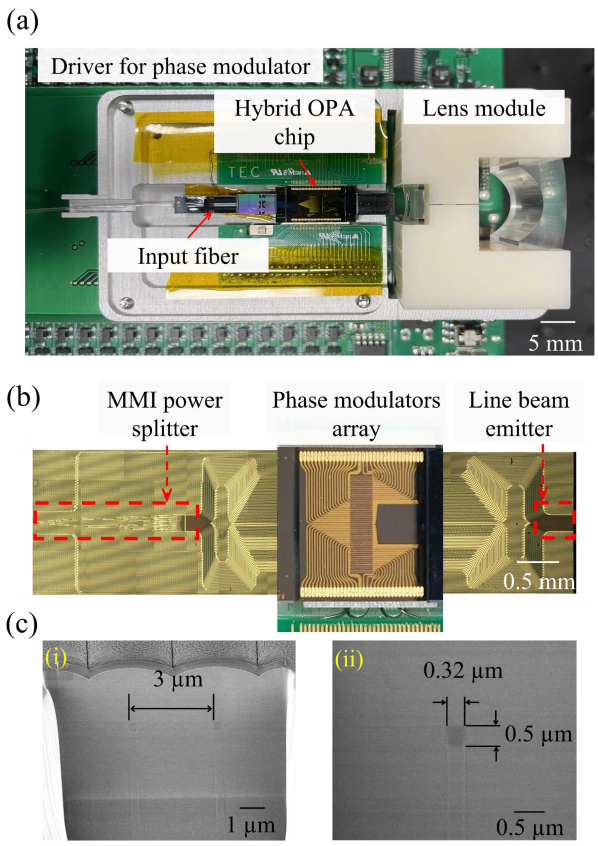

Fig. 6. (a) Assembled OPA transmitter inclusive of the hybrid OPA tethered to the lens module. (b) Microscope image of the manufactured hybrid OPA. (c) Cross-sectional FIB images of the line beam emitter made of SiN which consists of the tapered waveguides with a 3-μm spacing and 300-nm tip width.

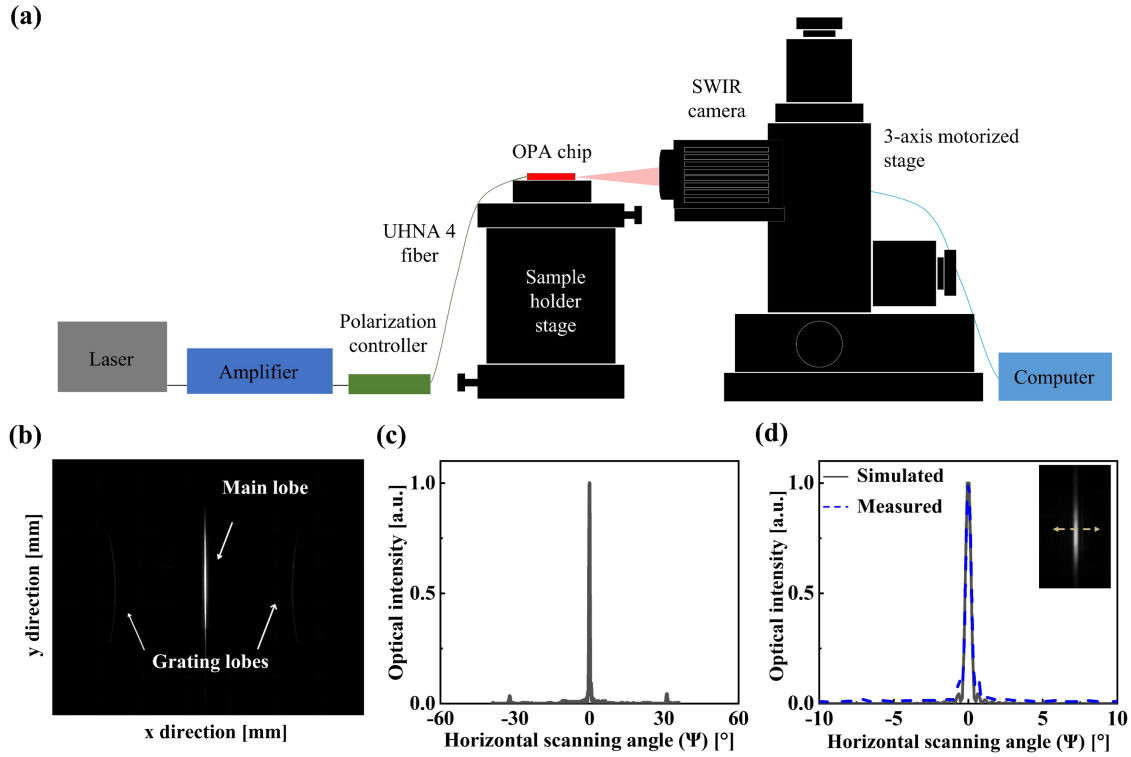

Fig. 7. (a) Schematic of the experimental setup for exploring the line beam performance. (b) Line beam profile captured by the SWIR camera. (c) Corresponding horizontal cross-section. (d) Comparison of simulated and measured results in terms of the horizontal beamwidth.

leading to beam scanning, as addressed in Appendix I. The SiN and polymer devices mentioned above were manufactured following a standard process for planar lightwave circuits. For the power splitter and line beam emitter made of SiN, a buried oxide (BOX) layer of 4 μm was formed on the silicon substrate. A SiN film with a thickness of 500 nm was deposited on the BOX layer via low-pressure chemical vapor deposition (LPCVD) and fully etched to create a waveguide pattern. A top cladding of 3.3 μm, made of the same oxide, was subsequently formed atop the patterned waveguide. The SiN chip was fabricated at Ligentec SA through a photonic damascene process. It is remarked that the power splitter and line beam emitter made of SiN were initially prepared in two separate chips, based on the same fabrication schemes. Then the two chips were successively aligned and bonded to the polymer phase modulator array via an ultraviolet (UV) curable epoxy, thus constructing a hybrid OPA chip. The completed chip was securely mounted in metal housing. The designed lens module, which was made of polymethyl methacrylate (PMMA) with a refractive index of 1.48 at $\lambda = 1550$ nm, was aligned to the line beam emitter at a distance of 2.5 mm. Fig. 6(c)-(i) and (ii) show focused ion beam (FIB) images of the cross-section of the fabricated line beam emitter, which comprises tapered waveguides with a tip width of 300 nm, uniformly spaced 3 μm apart. The fabricated SiN waveguide core was witnessed to be 500 nm in height and 320 nm in width.

The test setup for evaluating the manufactured OPA is depicted in Fig. 7(a). The incident light at $\lambda = 1550$ nm, generated by a tunable laser (Santec, WSL-110), was passed through an erbium-doped fiber amplifier. The input light was transverse electric polarized by a polarization controller and coupled to the OPA chip via an ultra-high numerical aperture fiber (Model UHNA4). A short-wave infrared (SWIR) camera (ABA-001IR-GE, AVAL DATA) mounted on a 3-axis motorized stage was used to appropriately capture the emitted beams exhibiting varying field-of-views. A SiN OPA incorporating a power splitter that was directly connected to a line beam emitter, without involving a phase modulator array, was separately prepared and examined in terms of the characteristics of line beams at a reference position when the scanning angle was 0°. Fig. 7(b) shows the captured beam profile of the line beam emitter, with a strong main lobe in conjunction with a pair of tenuous grating lobes on either side. The corresponding horizontal cross-section is shown in Fig. 7(c), where the grating lobes can be located at $\pm 31.1°$. Fig. 7(d) shows a comparison between the simulation and measurement results in terms of the beamwidth along the Ψ-direction, where the FWHM divergence angle was measured to be 0.4° as expected. The image in the inset is the far-field pattern captured by the SWIR camera. The SiN OPA was then tested in terms of the loss pertaining to the SSC and MMI-based power splitter as well as the propagation loss of the waveguides. Each SSC was witnessed to incur a coupling loss of 0.8 dB, whereas each MMI exhibited an excess loss of 0.2 dB, leading to a total insertion loss of 1.2 dB over a 6-stage MMI-based power splitter. The SiN waveguide exhibited a propagation loss of $\sim$0.2 dB/cm. The loss associated with the polymer modulator chip was characterized in a similar manner. Consequently, the hybrid-integrated OPA engendered a total insertion loss of $\sim$9

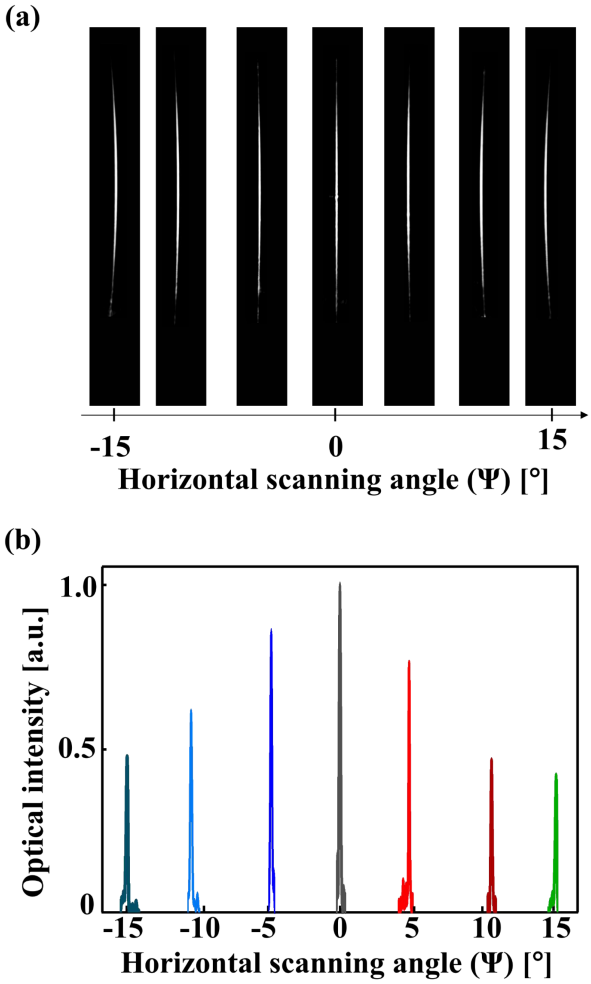

Fig. 8. (a) Captured beam profiles pertaining to the hybrid OPA chip under beam scanning. (b) Horizontal cross-sections of the beam profiles.

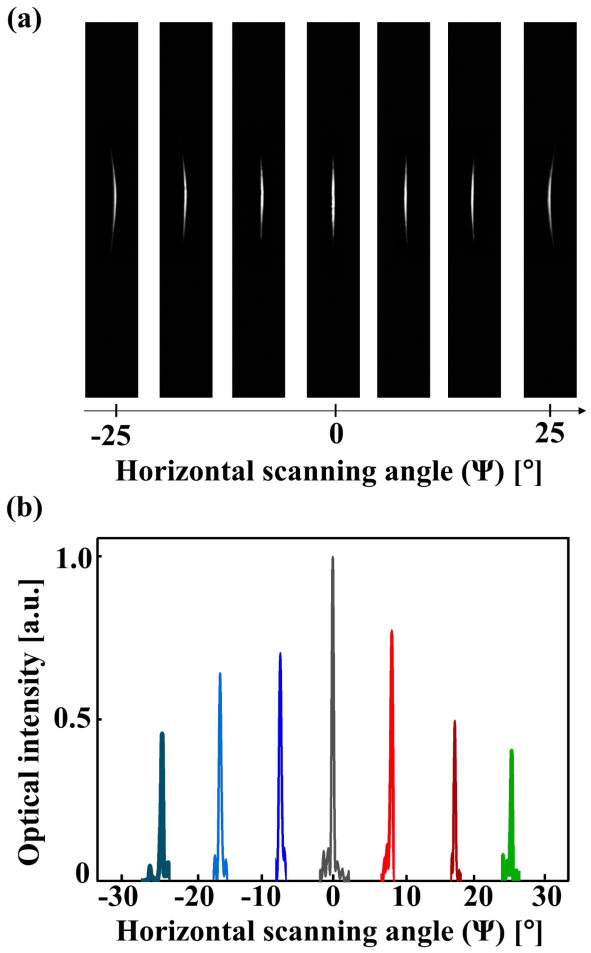

Fig. 9. (a) Captured beam profiles pertaining to the OPA transmitter under beam scanning. (b) Horizontal cross-sections of the beam profiles.

dB, which could be attributed to the fiber-to-splitter coupling (0.8 dB), splitter-to-modulator coupling (2 dB), power splitter (1.2 dB), polymer modulator array (1 dB), propagation loss (∼0.5 dB), and line beam emitter (0.5 dB). The remaining loss of ∼3 dB could be ascribed to an unwanted imperfect chip-to-chip bonding process, which will be improved by concocting a monolithically integrated SiN-polymer chip.

Next, the hybrid OPA chip was evaluated from the viewpoint of a line beam scanner. The beam scanning was practically achieved by adequately tuning the TO effect-induced phase shift across the phase modulators. By tailoring the $\Delta\varphi$ of the individual channels, the hybrid OPA was corroborated to readily fulfill line beam scanning. Fig. 8(a) shows the captured scanned images of line beams along the Ψ-direction. The achievable scanning range along the horizontal direction was approximately 30°, with a corresponding vertical FOV of 20°. The horizontal cross-sections of the line beam profile, as shown in Fig. 8(b) are seen to exhibit main lobe power variations of ∼3 dB. Finally, an OPA transmitter was assembled by combining the hybrid OPA chip with the lens module, with the working distance between them set at $d_1 = 2.5$ mm. The resulting line beam profiles are shown in Fig. 9(a). A beam scanning range of as large as ∼51° along the horizontal direction was ultimately obtained by thermo-optically inducing a phase gradient, testifying to an amplification factor of 1.7 facilitated by the lens module, as intended. In the meantime, a FOV of 5° was achieved along the θ-direction by adequately tailoring the tapered waveguides constituting the line beam emitter. The horizontal FWHM divergence of the scanned line beam appeared to stabilize in the vicinity of 0.6°. Fig. 9(b) shows the horizontal cross-section of the emitted beam profile, with $\Delta\varphi$ varying from $-180°$ to 180° in steps of 60°. The measured power variation of the main lobe was approximately 3.6 dB during beam scanning, which was commensurate with the simulation results. It is noted that the main lobe profiles were primarily monitored to inspect the beam scanning performance for both the OPA and the OPA transmitter containing the lens module. The completed OPA transmitter could be readily scanned through TO phase tuning, thus rendering FOVs ranging up to $51° \times 5°$ ($\Psi \times \theta$). As shown in Fig. 10, the vertical FOV was witnessed to remain stable in the vicinity of 5° over the course of beam scanning, unequivocally suggesting that the developed hybrid OPA transmitter is highly anticipated to play a pivotal role in embodying advanced LiDAR and wireless optical communication systems.

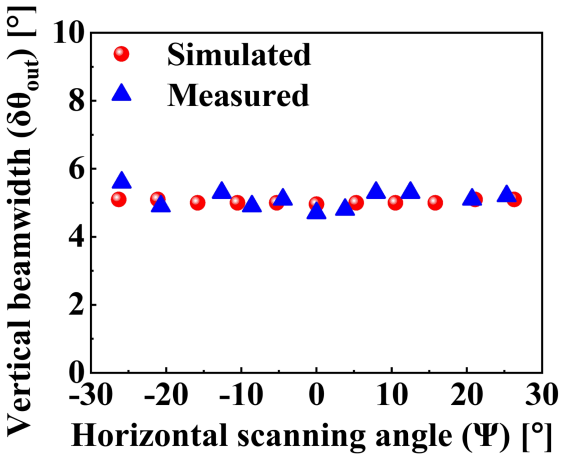

Fig. 10. Relationship between the vertical beamwidth ($\delta\theta_{\mathrm{out}}$) and horizontal scanning angle (Ψ) under the deployment of the lens module.

IV. Conclusion

A hybrid integrated OPA which exploits a line beam emitter based on a tapered waveguide array was successfully developed to fulfill efficient line beam scanning with flexible FOVs at a fixed wavelength of 1550 nm. A group of polymer phase modulators was combined with a power splitter and line beam emitter made of SiN via SSCs, thereby scanning a line beam along the horizontal direction by inducing phase gradients. The tapered waveguides constituting the line beam emitter have been varied in terms of their tip widths to flexibly tailor the vertical FOVs from 14° to 47°. A lens module was incorporated into the hybrid OPA, concurrently controlling and expanding the vertical and horizontal FOVs, respectively. The proposed transmitter, which comprises the hybrid OPA appended to the lens module, gave rise to adjustable FOVs ranging from 51° × 10.3° to 51° × 0.6°. Finally, the line beam scanning performance was experimentally validated with a vertical FOV of 5°. Our OPA transmitter will be an indispensable engine for realizing well-defined line beams, which are pivotal for materializing rapid scanning, long-distance operation, and adjustable FOVs toward advanced LiDAR applications.

Appendix
Characteristics of the Polymeric Phase Modulators

A phase modulator tapping into perfluorinated polymers has been exploited to conduct efficient line beam scanning with a low power consumption [25], [26], [27]. The cross-section of a TO phase modulator with a thin metal heater placed atop the waveguide is delineated in Fig. 11(a). Perfluorinated polymers (Model LFR available from ChemOptics, Co.) were spin-coated on a silicon substrate to form the core and cladding of the waveguide, exhibiting a refractive index contrast of 0.025. The phase modulator array was designed with a period ($\Lambda_{\mathrm{polymer}}$) of 50 μm to prevent thermal crosstalk between adjacent channels. The thickness of each layer pertaining to the polymer waveguide was $t_1 = 9$ μm, $t_2 = 3$ μm (core), and $t_3 = 6$ μm (lower cladding). The thermal characteristics of the phase

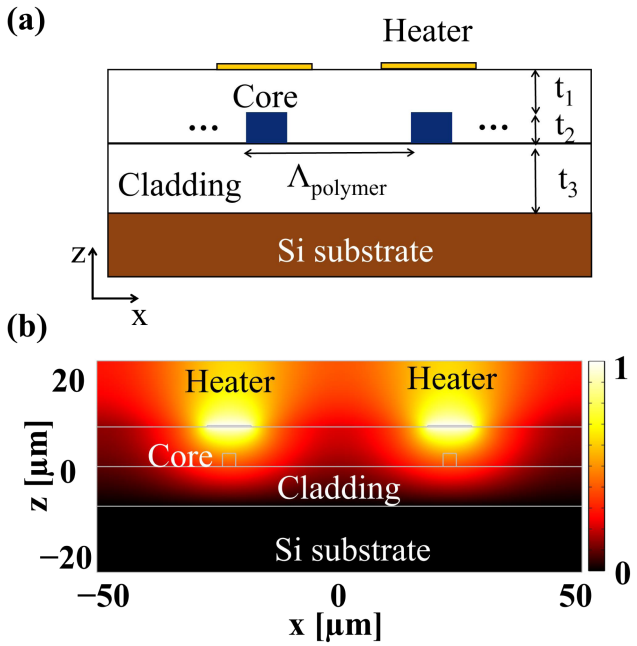

Fig. 11. (a) Cross-section of the TO phase modulators with the thin film heaters located on top of the waveguides. (b) Heat distribution of the polymer waveguides.

modulator were practically inspected using a test structure of a Mach-Zehnder interferometer. To impose TO phase tuning, the phase modulators were equipped with an Au thin-film heater of 10-μm width and 3-mm length. The thermal distribution pertaining to the waveguide, as shown in Fig. 11(b) was calculated using the finite element method (Optodesigner, Synopsys Inc.). The electrical power consumed to attain a π-phase shift was calculated to be as low as $P_\pi = 2.1$ mW, signifying the excellent TO property and thermal confinement of the adopted polymers which had thermal conductivity and TO coefficient of 0.2 W/mK and -2.5×10^{-4}/°C, respectively. The interferometer was deployed to investigate the power consumption of phase modulators experimentally, where the P_π was measured to be ~2.3 mW [26], [27], [28], [29].

Acknowledgment

The authors would like to acknowledge Ligentec SA (Lausanne, Switzerland) for the device fabrication.

References

[1] M. J. R. Heck, "Highly integrated optical phased arrays: Photonic integrated circuits for optical beam shaping and beam steering," *Nanophoton.*, vol. 6, no. 1, pp. 93–107, Jun. 2017.
[2] N. Dostart et al., "Serpentine optical phased arrays for scalable integrated photonic LiDAR beam steering," *Optica*, vol. 7, no. 6, pp. 726–733, Jun. 2020.
[3] J. C. Hulme et al., "Fully integrated hybrid silicon two dimensional beam scanner," *Opt. Exp.*, vol. 23, no. 5, pp. 5861–5874, Mar. 2015.
[4] S. Chung, H. Abediasl, and H. Hashemi, "A monolithically integrated large-scale optical phased array in silicon-on-insulator CMOS," *IEEE J. Solid-State Circuits*, vol. 53, no. 1, pp. 275–296, Jan. 2018.
[5] C.-S. Im, B. Bhandari, K.-P. Lee, S.-M. Kim, M.-C. Oh, and S.-S. Lee, "Silicon nitride optical phased array based on a grating antenna enabling wavelength-tuned beam steering," *Opt. Exp.*, vol. 28, no. 3, pp. 3270–3279, Feb. 2020.

[6] D. N. Hutchison et al., "High-resolution aliasing-free optical beam steering," *Optica*, vol. 3, no. 8, pp. 887–890, Aug. 2016.
[7] C. V. Poulton et al., "Long-range LiDAR and free-space data communication with high-performance optical phased arrays," *IEEE J. Sel. Topics Quantum Electron.*, vol. 25, no. 5, pp. 1–8, Sep./Oct. 2019, Art. no. 7700108.
[8] J. K. Doylend, M. J. R. Heck, J. T. Bovington, J. D. Peters, L. A. Coldren, and J. E. Bowers, "Two-dimensional free-space beam steering with an optical phased array on silicon-on-insulator," *Opt. Exp.*, vol. 19, no. 22, pp. 21595–21604, Oct. 2011.
[9] M. Raval, A. Yaacobi, and M. R. Watts, "Integrated visible light phased array system for autostereoscopic image projection," *Opt. Lett.*, vol. 43, no. 15, pp. 3678–3681, Aug. 2018.
[10] C. V. Poulton et al., "Large-scale silicon nitride nanophotonic phased arrays at infrared and visible wavelengths," *Opt. Lett.*, vol. 42, no. 1, pp. 21–24, Jan. 2017.
[11] W. D. Sacher, Y. Huang, G.-Q. Lo, and J. K. S. Poon, "Multilayer silicon nitride-on-silicon integrated photonic platforms and devices," *J. Lightw. Technol.*, vol. 33, no. 4, pp. 901–910, Feb. 2015.
[12] B. Bhandari, C.-S. Im, O. R. Sapkota, and S.-S. Lee, "Highly efficient broadband silicon nitride polarization beam splitter incorporating serially cascaded asymmetric directional couplers," *Opt. Lett.*, vol. 45, no. 21, pp. 5974–5977, Nov. 2020.
[13] N. A. Tyler et al., "SiN integrated optical phased arrays for two-dimensional beam steering at a single near-infrared wavelength," *Opt. Exp.*, vol. 27, no. 4, pp. 5851–5858, Feb. 2019.
[14] Q. Wang, S. Wang, L. Jia, Y. Cai, W. Yue, and M. Yu, "Silicon nitride assisted 1×64 optical phased array based on SOI platform," *Opt. Exp.*, vol. 29, no. 7, pp. 10509–10517, Mar. 2021.
[15] D. Kwong et al., "Corrugated waveguide based optical phased array with crosstalk suppression," *IEEE Photon. Technol. Lett.*, vol. 26, no. 10, pp. 991–994, May 2014.
[16] S. A. Miller et al., "Large-scale optical phased array using a low-power multi-pass silicon photonic platform," *Optica*, vol. 7, no. 1, pp. 3–6, Jan. 2020.
[17] P. Wang et al., "Design and fabrication of a SiN-Si dual-layer optical phased array chip," *Photon. Res.*, vol. 8, no. 6, pp. 912–919, Jun. 2020.
[18] C.-S. Im et al., "Hybrid integrated silicon nitride–polymer optical phased array for efficient light detection and ranging," *J. Lightw. Technol.*, vol. 39, no. 13, pp. 4402–4409, Jul. 2021.
[19] Y. Zhang et al., "Sub-wavelength-pitch silicon-photonic optical phased array for large field-of-regard coherent optical beam steering," *Opt. Exp.*, vol. 27, no. 3, pp. 1929–1940, Feb. 2019.
[20] M. R. Kossey, C. Rizk, and A. C. Foster, "End-fire silicon optical phased array with half-wavelength spacing," *APL Photon.*, vol. 3, no. 1, Dec. 2017, Art. no. 011301.
[21] W. Xu, L. Zhou, L. Lu, and J. Chen, "Aliasing-free optical phased array beam-steering with a plateau envelope," *Opt. Exp.*, vol. 27, no. 3, pp. 3354–3368, Feb. 2019.
[22] D. Wu, Y. Yi, and Y. Zhang, "High-efficiency end-fire 3D optical phased array based on a multi-layer Si_3N_4/SiO_2 platform," *Appl. Opt.*, vol. 59, no. 8, pp. 2489–2497, Mar. 2020.
[23] M. C. Shin et al., "Chip-scale blue light phased array," *Opt. Lett.*, vol. 45, no. 7, pp. 1934–1937, Apr. 2020.
[24] B. Bhandari, C.-S. Im, K.-P. Lee, S.-M. Kim, M.-C. Oh, and S.-S. Lee, "Compact and broadband edge coupler based on multi-stage silicon nitride tapers," *IEEE Photon. J.*, vol. 12, no. 6, pp. 1–11, Dec. 2020, Art. no. 6602511.
[25] T.-H. Park, S.-M. Kim, S.-H. Park, J.-K. Seo, H.-G. Lee, and M.-C. Oh, "Polymer waveguide WDM channel selector operating over the entire C and L bands," *Opt. Exp.*, vol. 26, no. 13, pp. 16323–16332, Jun. 2018.
[26] S.-M. Kim, E.-S. Lee, K.-W. Chun, J. Jin, and M.-C. Oh, "Compact solid-state optical phased array beam scanners based on polymeric photonic integrated circuits," *Sci. Rep.*, vol. 11, no. 10576, pp. 1–9, May 2021.
[27] Z. Zhang and N. Keil, "Thermo-optic devices on polymer platform," *Opt. Commun.*, vol. 362, no. 1, pp. 101–114, Mar. 2016.
[28] M.-C. Oh et al., "Polymeric optical waveguide devices exploiting special properties of polymer materials," *Opt. Commun.*, vol. 362, no. 1, pp. 3–12, Mar. 2016.
[29] E.-S. Lee, K.-W. Chun, J. Jin, and M.-C. Oh, "Frequency response of thermo-optic phase modulators based on fluorinated polyimide polymer waveguide," *Polymers*, vol. 14, no. 11, May 2022, Art. no. 2186.